



HAL
open science

First assessment of recent tectonics and paleoearthquakes along the Irtysh fault (eastern Kazakhstan)

S. Baize, K. Reicherter, A. Avagyan, A. Belyashov, E. Pestov, E. Vittori, A.
Arakelyan, K. Decker

► To cite this version:

S. Baize, K. Reicherter, A. Avagyan, A. Belyashov, E. Pestov, et al.. First assessment of recent tectonics and paleoearthquakes along the Irtysh fault (eastern Kazakhstan). *Geomorphology*, 2019, 326, pp.90-106. 10.1016/j.geomorph.2018.09.013 . hal-02521616

HAL Id: hal-02521616

<https://hal.science/hal-02521616>

Submitted on 12 Oct 2021

HAL is a multi-disciplinary open access archive for the deposit and dissemination of scientific research documents, whether they are published or not. The documents may come from teaching and research institutions in France or abroad, or from public or private research centers.

L'archive ouverte pluridisciplinaire **HAL**, est destinée au dépôt et à la diffusion de documents scientifiques de niveau recherche, publiés ou non, émanant des établissements d'enseignement et de recherche français ou étrangers, des laboratoires publics ou privés.



Distributed under a Creative Commons Attribution - NonCommercial - NoDerivatives 4.0
International License

First assessment of recent tectonics and paleoearthquakes along the Irtysh fault (eastern Kazakhstan)

Stéphane Baize (1), Klaus Reicherter (2), Ara Avagyan (3), Andrey Belyashov (4), Evgeniy Pestov (4), Eutizio Vittori (5), Avetis Arakelyan (6), Kurt Decker (7)

(1) IRSN Institut de Radioprotection et de Sécurité Nucléaire, Fontenay Aux Roses, France,
stephane.baize@irsn.fr

(2) Neotectonics and Natural Hazard, RWTH Aachen University, Aachen, Germany, k.reicherter@nug.rwth-aachen.de

(3) Institute of Geological Sciences, National Academy of Sciences of Armenia, Yerevan, Armenia
avagn1064@gmail.com

(4) Institute of Geophysical Research, Kurchatov, Kazakhstan, abelyashov@gmail.com and pestov@igr.kz

(5) Dipartimento per il Servizio Geologico d'Italia, Istituto Superiore per la Protezione e la Ricerca Ambientale, Rome, Italy, eutizio.vittori@isprambiente.it

(6) Armenian Association of Seismology and Physics of the Earth, Yerevan, Armenia,
vitoarakel@yahoo.com

(7) Department of Geodynamics and Sedimentology, University of Vienna, Vienna, Austria,
kurt.decker@univie.ac.at

Abstract

The Asian plate interiors are known to have host strong earthquakes with magnitudes up to $M \approx 8$ in recent history, especially around the border area between Mongolia, Kazakhstan, China and Russia (e.g., $M7.3$ Chuya earthquake, 2003). Their recurrence times seem to be long, because of the relative low slip rates (less than 1 mm/y) of the faults which caused them.

In this study, we focus on a large inherited fault zone (namely the Irtysh Fault Zone) with no historical earthquakes larger than $M6$, to test whether this structure could have generated surface-rupturing events during the last thousands of years, like some other historically silent similar faults of

cratonic southern Kazakhstan did in pre-historic times. To do so, we use tectonic-morphological analyses of satellite images and trenching across several fault portions to detect potential paleoearthquakes.

The Irtysh Fault Zone (IFZ) is a 250+ km long basement set of faults that marks a major tectonic block boundary between different units with Paleozoic magmatic rocks and thick deposits of Late Paleozoic age. The formation of the IFZ dates back into the Late Paleozoic times during collision between Siberia-Kazakh cratons and it was repeatedly reactivated in later times (e.g., Oligo-Miocene). The Quaternary activity of the Irtysh Fault Zone has never been addressed in modern studies and, in this study, we document for the first time that the IFZ is an active fault and is a potential source of large earthquakes in easternmost Kazakhstan. Our analyses actually revealed, at different spots along the IFZ, the occurrence of a set of lineaments offsetting lithologies or deflecting streams and other landscape features. Trenching sites across those lineaments eventually confirmed that they were active fault strands and in some trenches, ^{14}C -dated Holocene-Late Pleistocene deposits are clearly faulted. Those recent deposits include organic soils, loess layers and colluvium directly overlying the Paleozoic rocks. Our findings lead to the conclusions that the IFZ is clearly active along several strands of its trace in bedrock. During the Holocene, it hosted earthquakes with surface rupture individual displacements of up to 1.5 meters, suggesting events with a magnitude around $M \approx 7$.

However, our investigations do not allow to confident estimation of slip rates: we propose for one fault section parallel to the main fault a preliminary estimation of ~ 0.22 mm/y vertical displacement rate, based on a single trench. Based on regional morphoclimatic arguments and landscape features offsets, we also propose a first assessment of the lateral slip rate along the major fault between 0.3 and 0.5 mm/y.

Additional investigations should be undertaken to refine surface fault mapping, the paleoearthquake calendar, the slip rate, and potential along-strike evolution, in order to constrain future seismic hazard analyses with fault models in this region of Eastern Kazakhstan.

Keywords: tectonic geomorphology; paleoseismicity; eastern Kazakhstan, Irtysh fault, stable continental region

1. Introduction

Large (M 7) to great (M 8) earthquakes have occurred in Asian plate interiors, including places with low strain rates. For instance, a sequence of four M ~8 earthquakes shook Mongolia and China in 1905, 1931, and 1957 (Molnar and Qidong, 1984). Further west, the Russian Altai Mountains were shook in 2003 by the Mw 7.2 Chuya earthquake generated on a 1 mm/y slip rate active fault (Dorbath et al., 2008), leading to a complex surface rupture (Lunina et al., 2008). The relationship between those big earthquakes and Central Asia surface faults has been demonstrated through geological mapping of surface ruptures and paleoseismological investigations (e.g., Rizza et al., 2015, for Mongolia Faults). In plate interiors of southern Kazakhstan, recent studies documented two NW-SE inherited and seismically silent faults (namely the Dzhungarian and Lepsy faults), with right-lateral faulting activity and paleoearthquake evidence (Campbell et al., 2013, 2015). Farther north close to the Russian border, the Irtysh Fault Zone (IFZ) is another similar NW-SE inherited fault zone, with no significant historical earthquakes, for which the question of recent tectonic activity has not been addressed. In this study, we use surface information such as satellite images and trenching data to test whether the IFZ could have been active in the last thousands of years and potentially responsible for surface-rupturing events, such as the Dzhungarian and Lepsy faults.

The IFZ is located in easternmost Kazakhstan; it stretches along the Irtysh River south of the Rudny Altai Mountains, near the borders with Russia, China, and Mongolia. The fault zone runs

parallel to the Bukhtarma reservoir dammed by a hydroelectric power plant, passes through the populated area around Öskemen city (Kazakh name; Ust-Kamenogorsk in Russian; > 300,000 inhabitants in 2012), the administrative center of the Eastern Kazakhstan Region, then stretches to the northwest to Siberia along the Irtysh River plain. The study area is far north of the active range of Tien-Shan in southern Kazakhstan where high strain rates correlate with historical large earthquake locations (e.g., 1911 M 7+ Chon-Kemin or 1992 M 7.3 Suusamyr earthquakes, described respectively by Arrowsmith et al., 2017, and Ghose et al., 1997) and high seismicity rates. Grützner et al. (2017) recently documented the seismotectonic activity of Tien Shan Faults bounding the Kazakh platform to the south, close to Almaty.

Based on work carried out in 2014 and 2015, we provide new insights on the active tectonics of the area and give preliminary assessment of parameters for the fault zone, such as first-order mapping of the fault, magnitude of past earthquakes and a preliminary assessment of slip rate. Remote sensing analyses and field missions have allowed pinpointing the key tectonic features of the study region southeast and northwest of Öskemen, southward to Alibay, and northward to Predgornoje. The geomorphological evidence, such as vertical and horizontal displacement of slopes and gullies, reveals a clear Quaternary fault activity, which generally fit the faults mapped on the geological sheets (Bekzhanov et al., 2000). The potential Quaternary activity was confirmed after our analysis of the trenches that revealed the occurrence of Holocene earthquakes. Morphotectonic features are more prominent around and south of Öskemen, especially along the Bukhtarma Lake shoreline and nearby Öskemen. With these results, we could roughly constrain the paleo-event magnitudes, the ages of those surface-rupturing earthquakes, and very roughly a broad idea of their return period, all of these being crucial parameters for seismic hazard analyses.

2. Geological and geodynamic background

2.1. Tectonic history

The Rudny Altai Mountains magmatic arc (northeast of IFZ) and Kalba–Narym fore-arc turbidite ensemble (southwest of IFZ) developed during oblique subduction of the ancient Zaysan ocean floor (Chara) under the Siberian margin (Fig. 1). Basically, the IFZ today juxtaposes the Kalba-Narym terrane on the southwest, composed of Paleozoic granitoids and turbidites with local sequence of ophiolites revealing the subduction of Kazakhstan Block beneath Siberia before their collision, against the Rudny-Altai terrane to the northeast, composed of Paleozoic sedimentary series and Mesozoic granitoids.

Based on zircon U/Pb ratios, apatite fission track and fault kinematic data, Glorie et al. (2012) provided a complete tectonic history of the IFZ. At the end of the Paleozoic, the collision of Siberia and Kazakhstan blocks was completed, initiating left-lateral displacements along the IFZ. A Late Cretaceous uplift and related denudation/peneplanation of the Altai basement rocks was followed by the cease of tectonic activity (late Mesozoic–early Cenozoic). The thermal history of the granitoids surrounding the IFZ indicates a renewed period of activity along the ISZ during the Oligocene and Mio–Pliocene as a response to subsidence of the Zaysan basin (located south of Fig. 1). The late Plio-Pleistocene phase of Altai Mountain building coincides with new right-lateral faulting conditions.

2.2. Recent tectonics

From the geodynamic viewpoint, the study region is well north of the active Tien Shan Range (TS), which accommodates two thirds (~20 mm/y) of the Indian-Eurasian convergence north of the Himalaya plate boundary (Fig. 1). Far north of the plate boundary, a set of large NNW-SSE dextral (e.g., MA: Mongolian Altai-labeled fault) or E-W sinistral strike-slip fault zones have developed in the Eurasian plate interiors, including the IFZ. The area surrounding this last can clearly be considered as an intraplate region, which is confirmed by the paucity of $M > 5.5$ earthquakes since 1761, date of the largest historical earthquake ($M \sim 6.5$) (Fig. 2). A recent calculation of displacement field in Central Asia (Zubovich et al., 2010) yields an ambiguous pattern around the IFZ (Fig. 2). The GPS sites show relative velocities with respect to Eurasia mainly in the strike of the IFZ, with values between 0

and 4 mm/y to the northwest. No clear deformation pattern appears from that GPS velocity field. Stress indicators as reported by the World Stress Map (Fig. 1), however, strongly suggest that the IFZ would deform as a right-lateral fault, which is confirmed by the long-term morphology (see hereafter). All current tectonics information shows that the IFZ region is a slowly deforming area. The strain rate (namely the second invariant of the strain rate tensor) is low, in the range of 1 to 5 nanostrain (10^{-9}) per year (Kreemer et al., 2014).

Moho discontinuity is at around 50 km depth in the IFZ region (Petrov et al., 2016). We have no direct information around the fault zone about the seismogenic depth that could be mobilized during future events, and we therefore have no tight control of the maximum width of this potential extreme earthquake rupture. A good proxy for seismogenic thickness is the locking depth that can be inferred from geodesy. Unfortunately, no such information is available in Kazakhstan. Smith-Konter et al. (2011) concluded for California that the seismogenic thickness best matches the locking depth when determined at the 95% cutoff depth in seismicity: here we use the national instrumental catalogue provided by the Institute of Geophysics of Kazakhstan to infer this critical parameter, which eventually is about 30 km. This result is consistent with the seismicity depth distribution obtained by Sloan et al. (2011) for the Tien Shan forelands (including the Kazakhstan platform) in a continental study based on teleseismic data.

3. Morphological signature of the Irtysh Fault activity

Before developing a trenching campaign, we conducted a morphotectonic analysis along the Irtysh Fault Zone trace. We basically used Google Earth and high-resolution satellite images available online on the ESRI World Imagery website (<http://services.arcgisonline.com/arcgis/rest/services>). The IFZ cuts through a hilly landscape dominated by erosion upstream Öskemen, and by aggradation downstream. Southeast of Öskemen, the river is currently incising low relief bedrock mounds and hills; to the northwest, the relatively flat area around the fault zone has been extensively buried

either by the meandering or anastomosing river or by aggradation of aeolian sediments during cold phases of the Quaternary. The Irtysh River could easily avulse, and this powerful river probably could erase or mask a lot of fault activity evidence. The impact on tectonic feature preservation is probably significant because of the slow slip rate of fault. We also underline that the inherited bedrock structure, developed during ancient tectonic phases, has a strong impact on drainage features, deflection of streams, generation of scarps at lithological contacts, etc., and we therefore had to be very careful when interpreting the landscape in terms of active tectonics.

In various places, we observe sharp and linear traces with a clear and consistent imprint on the modern drainage network suggesting recent tectonic activity, including linear mountain front, triangular facets, stream deflections, slope gradients and breaks, beheaded channels, shutter ridges, etc. We report here four particular areas including the most compelling morphological evidence of recent activity, namely the southeast, central southeastern, central northwestern, and northern areas. For each area, Fig. 3 to 8 show the raw satellite images with some annotations, and a basic morphological interpretation is reported as sketches in the supplementary material. We also used the oblique to perpendicular-to-fault linear morphological features (valley slopes, incised channels) to measure the right-lateral offsets associated with fault activity; a map locating the measurement points is provided in the supplementary material. For most of the sites under consideration, we picked two extreme values to represent the variability of measurement depending on which landscape features were matched on both sides of the fault. Those tectonic lineaments were then tracked to place paleoseismological trenches, which were selected at the end, balancing their accessibility and their potential content in recent sediments (for dating events).

3.1. Alibay (southeast) area

Two subparallel lineaments are documented along the northeastern shoreline of the Bukhtarma Reservoir lake. Figure 3 presents a close-up of those lineaments along the shoreline. The first sharp trace, continuous over more than 4 km, is at the mountain front to the northwest, then extends

inside a longitudinal perched valley where its trace is particularly compelling. Along most of its course, the segment location does not seem to be influenced by lithological changes as suggested by the satellite image texture. A large alluvial fan apex is dextrally offset by ~30 m, and we observe that the long-term alluvial fans at the toe of the mountain front and the fault are asymmetric. This asymmetry can be explained by the long-term right-lateral offset of the upstream incised drainage network with respect to the erosional/aggradation area (alluvial fan). At the fanhead, terrace risers on the southeast side of the stream are generally in erosion ('leading edge' terraces), which also supports right-lateral offset. The second trace, to the southwest, is less continuous, appears to be partly controlled by lithological changes, and does not seem to cut the alluvial fan. This lineament bounds to the north another asymmetrical alluvial fan that can be, besides a clear fault signature in the bedrock, a sign of Quaternary tectonic activity.

3.2. *Bukhtarma reservoir (central southeastern) area*

Along the northwestern coast of the Bukhtarma Reservoir, between the settlements of Oktyabrsky and Berezovka, a major lineament follows a very low sinuosity and almost rectilinear mountain front (Fig. 4), which can be followed over ~20 kilometres. This front is defined by a lithological contact between green metamorphic rocks to the northeast, and different types of gneiss and magmatic rocks to the southwest, but it largely influences the drainage pattern as well. The lineament can be mapped on satellite images and was observed at several sites along the slope during field inspection. It corresponds to a marked uphill increase of stream gradients. In addition, the associated scarp shows steep triangular facets. Beheaded valleys terminating at the lineament are common, and some of these valleys are located right in front of facets. At several places the lineament corresponds to the contact between basement rock and scree/colluvium. The paleoseismological information on the main fault strand was acquired at the point labeled *Railway*, an outcrop illustrating the surface faulting of recent sediments, as detailed later.

Numerous streams are clearly deflected at the lineament, but the restoration is often complicated by the change in stream density that increases below the lineament, probably because of a change in basement lithology. As in the Alibay area, we observe that large-scale alluvial fans in the area present a clear asymmetry (black arrows on Fig. 4) consistent with a long-term dextral component of the IFZ. We observe, from satellite images, a match between the drainage features on both sides of a 1-km-scale portion of the lineament (Fig. 5). The true right edges (southwest) of those small-scale incised features indicate a systematic dextral displacement. In a dextral-moving environment, they have been preserved from erosion ('trailing edges') and are the most reliable features that can be used to determine the deflection, which ranges from 15 to 35 m, suggesting a recent (Holocene-Pleistocene) activity. On Fig. 5, we provide a range of values covering alternative measurements of the same right-bank features, based on different initial angle. On that side of the Railway site, the mountain front lineament is paralleled by another 4-km-long lineament several tens of meters southwest, independent from lithological changes (Fig. 5). The latter does not show any clear lateral deflection of the stream network and it could correspond to a fault segment with only vertical component. Farther southwest from the master fault (1 km), another 3-km-long WNW-ESE lineament delineates a relatively uplifted block to the south (Fig. 4): we documented paleoseismological activity along this fault strand in trench-1. Southeast of the Railway site toward the cement plant, the fault signature along the lineament is particularly obvious (Fig. 6), marked by a low shutter ridge in front of a streamlet. Close to the plant, we observed other evidence of beheaded streams and several deflections of drainage that evoke dextral offsets, in many cases compensated by later captures. One of these deflections provide an estimation between 33 and 70 m of dextral offset.

3.3. *Öskemen (central northwestern) area*

Five to fifteen kilometres ESE of Öskemen, two sharp lineaments crosscut the bedrock hills and apparently deflect landscape features. These scarps, striking almost parallel to the Irtysh fault, are

well off the geological trace of the IFZ and do not correspond to previously mapped fault segments. However, they could connect to the east to the mapped Irtysh fault where several deeply incised valleys seem dextrally offset by ~100-150 m, north of the Ermanovka locality (see hereafter).

Considering the southern lineament of this area, the geological and morphological mapping proves that this feature is a tectonic fault offsetting the bedrock amphibolites and is not caused by lithological contact or foliation trend (Fig. 7, top). This lineament, extending over 5 km with N 110° strike, is very sharp and linear; and the scarp locally marks the contact between basement rock and alluvial sediments. The structure potentially associated with this feature seems to dextrally offset a bedrock layer (the westernmost dashed line on the top image of Fig. 7) and landscape features as well, such as bedrock-incised creeks and valley slopes. The smaller-scale features are dextrally displaced in the range of 15 to 30 m. These values must be considered as apparent because the kinematics of this fault line is probably oblique, including a certain vertical component as suggested by the general topography.

The northern lineament stretches over 1.5 to 3 km from the eastern suburbs of Öskemen toward the dam (Fig. 7, lower illustration). Geological and structural data obtained at that site strongly support the hypothesis that this structure is tectonic and active during recent times (Pleistocene to Holocene). Bedrock is coarse granite to the southwest, which is overlain by foliated dark gneiss to the northeast. The lithological contact there dips about 45° toward northeast. The change in slope gradient along the scarp as well as the steepening of stream profiles upstream of the fault (knickpoints) could be at least partially because of lithological change. However, the gathered structural data (slickensides, dykes with quartz mylonites) prove the occurrence of a subvertical dextral strike-slip fault that is thought to have been reactivated in the late Quaternary, as suggested by the morphological impact: stream deflections, shutter relief along fault with local pond and sediment aggradation occurrence, rare beheaded short valleys. Determination of deflection amount is not easy in this specific case because of the irregular shape of the drainage network (mainly on the

downstream block): the two indicated values on Fig. 8 correspond to the values measured using the left and right valley edges (see supplementary material). If deflections are of tectonic origin, the dextral component of offset varies there between 45 and 160 m.

3.4. Predgornoje (northern) area

Morphological evidence of fault activity are very tenuous in this area, which is largely under Irtysh River avulsion influence. Two parallel lineaments were, however, perceptible in the morphology of basement hills: the first northeast of the river with a slight slope gradient (parallel to the basement bedding), and the second southwest of the river within the Tavia Hills (which emerges in the middle of the Irtysh alluvial plain) (Fig. 8). The latter lineament is more important and seems to have an impact on the alluvial fan surface (see hereafter).

4. Paleoseismological survey

4.1. Methods

The trenches were excavated with a backhoe (Institute of Geophysics of Kurtchatov) with an ~50-cm-wide bucket, which failed during the very last trench in the Predgornoje area without prejudicing the completion of the study. Trenches were cleaned by hand and gridded by the authors and personnel from IGR. Geological analyses, logs, and sampling were performed by the authors of this paper. The coordinates of outcrop and trenches are listed in Table 1. In the main text, we provide geological logs of the sections, which are complemented by pictures in the supplementary material. Soil samples were gathered at critical places in the sections, and ^{14}C dating was carried out by Beta Analytic Laboratory in Miami, USA. Calibrated ages were obtained using the classical IntCal13 calibration curve (Reimer et al., 2013). We stress that the timing of paleoseismic events, exposed later in our geological interpretations, bears a significant uncertainty because of the use of bulk soil samples.

Preliminary geophysical surveys were locally performed in order to find in the upper geological layers, above the Paleozoic bedrock and soft Cenozoic deposits, the traces of existing faults to define their accurate location and geometry when nonvisible in the morphology. Those pretrenching studies were mandatory for trench siting in the Öskemen urban area and close agricultural sites (Trench-2) and complemented the morphological analysis (see supplementary material), which was not completely conclusive at that place. We applied seismic and GPR surveys.

4.2. *Railway cut*

A first outcrop was unearthed in August 2014 at the scarp base of the Irtysh fault along the Railway (Railway cut section, see coordinates in Table 1). This outcrop exposed faulted recent deposits, just north of the Bukhtarma dam along the railway. Owing to the limited time and the logistical issues, the site was not excavated with a motorized excavator; only a quick cleaning was carried out by hand, exposing only a limited stratigraphic section (5 m wide and nearly 4 m high). The section evidenced colluvial deposits in tectonic contact with the basement rocks. A reference grid (1 x 1 m) was applied to help in mapping the main exposed features (Fig. 9).

The bedrock (B) is a metamorphic schist, with foliation nearly parallel to the fault trend and dipping northeast. This rock is brought to an abrupt subvertical contact with late Quaternary slope deposits through half-meter-wide fault zone of highly crushed bedrock, often grading into fault gouge, locally bounded to the left by rock slates. The section starts with well-packed colluvium partially weathered and caliche-coated, including thin and flat small sheets of phyllite (horizon '5'). The overlying horizon ('4') is interpreted as a possible wedge of infilling material eventually sheared by the fault zone. Above it, following an undulated contact surface, we find a compact, slightly cemented slope deposit with centimeter-long fragments of bedrock and sand (horizon '3'). It appears to taper off the fault, which suggests it could be a colluvial wedge. Above it, an undeformed and post-deformation slope deposit (horizon '2') is overlain by the current soil (horizon '1'). We sampled only two places for radiocarbon dating to provide a rough idea of the date of the last surface-

rupturing event in the section. The upper layer ('2') yielded an age of calibrated date of A.D. 775-970; whereas the colluvial wedge ('3'), assumed to be the 'event horizon', yielded a 1225-1045 B.C. date (which can be considered to be a minimum date of the earthquake). We have no direct access to the event-related offset. However, we use the colluvial wedge thickness as an indirect indicator of per-event displacement (McCalpin, 2009), applying the rule of thumb *initial scarp height = 2 x maximum colluvial thickness*. In our case, a maximum thickness of 0.5 m leads to a 1-m-high scarp associated with an $M_w = 6.7-6.9$ earthquake (applying the *all type* event scaling relationship of Wells and Coppersmith, 1994). Considering that the earthquake rupture may have had a lateral component on this oblique fault (see section 3), this magnitude value must be considered as a minimum. Another older earthquake could have occurred before the '3' event, considering that the '4' horizon could also be a colluvial wedge; we have no dating constraint on that layer. In that case, two surface-rupturing events could have occurred.

4.3. Bukhtarma (central southern) area trench

The morphological analysis gives evidence of a nice lineament at the base of the mountain front, which probably constitutes the major fault. Thanks to the Railway cut, we document a Holocene surface-rupturing earthquake on that main fault strand after the first campaign in August 2014 (see above). During the second trenching fieldwork campaign between 24 and 28 August 2015, we decided (after considering time restrictions, technical facilities, and site examination results) to excavate a deeper trench across a secondary and antithetic scarp (Fig. 10) off the major fault scarp at 1 km to the south.

The main N-S trench (trench-1) was dug perpendicular to the scarp and evidenced by recent colluvium deposits in tectonic contact with the granitoid bedrock (subvertical fault). Two smaller trenches were additionally excavated to complete our information. In the main trench, four main geological units have been identified (Fig. 10). The oldest layer above the granitic bedrock ('4') in the trench is a colluvium of yellowish color ('3'). This colluvium is overlain by brownish clayey sand ('2')

then a black organic-rich soil horizon ('1'). The granitic bedrock (Permian) shows WNW-ESE trending subvertical foliation.

We interpret the trench section as the result of two surface faulting events (Fig. 10). The first and most important event has displaced vertically the granitic bedrock. The general arrangement of the geological units shows that the basement top surface is gently dipping on both sides (footwall and upper hanging wall) of the fault, which allows for reconstructing a $\sim 20^\circ$ northward-dipping slope before the event. Assuming then large (> 1 m) vertical displacement of that surface, we define afterward a phase of scarp degradation that we assume to start more or less with the deposition of the colluvium deposits (7455-7185 B.C.) which, in our model, slightly post-dates the deformation event. Afterward, the slope is graded after deposition of the wedge-shaped colluvium ('3'). No striation could be observed on the fault plane; but from the morphological signature, we estimate that the fault is mainly dip slip, with maybe a slight right-lateral component. The resulting (mainly) vertical displacement is evaluated by ~ 1.5 m as shown on Fig. 10 and in the supplementary material. In an assumed single earthquake, the magnitude could have reached 6.8 to 7.1 according to the Wells and Coppersmith (1994) empirical relationship for all-type earthquakes. The second and last recorded faulting event affects the unconsolidated sediments ('2' horizon) and the base of modern soil ('1' horizon); this event has not properly generated a recognizable colluvial wedge, maybe because of the nature (organic soil) exposed by the low relief scarp. The estimated vertical displacement is about 18-26 cm, and the corresponding magnitude M_w is estimated 6.1 to 6.4.

The first event is clearly older than the '2' layer (3630-3375 B.C.) and we assume that it occurred shortly before the 7455-7185 B.C. sample of the '3' layer. The last recorded event (18-26 cm of vertical offset) is bracketed by the two modern soil samples (815-780 B.C. and A.D. 720-895), occurring then between 815 B.C. and A.D. 895. Considering that those two events have offset the base of the Holocene by $\sim 1.5 + 0.3$ m during the last 8000 years, a rough vertical slip rate of 0.22 mm/y is inferred. We stress that this estimation is only based on two events and then should clearly

be considered with caution. A more complete stratigraphic recording of paleoearthquakes would be necessary to infer a robust estimation.

4.4. *Öskemen area trench*

Three trenches have been placed north of Öskemen (29 August – 6 September 2015) in a WNW-ESE dry valley along a mapped fault, where the drainage forms a deep valley just a few meters behind the ridge to the southwest (Fig. 11). Actually, this morphologic feature resembles a mini-graben between two minor fault strands of the IFZ. This morphological feature has been detected by satellite image analysis, and trenches were precisely located after surface geophysics (see supplementary material for details). Two out of three trenches revealed surface deformation.

A first trench (trench-2) was excavated across the western segment, where schists and minor granitic rocks crop out, with a length of more than 26 m. We encountered ~2-m-thick Holocene loess/silt deposits covered by modern soil (Fig. 11). Bulk ^{14}C dating provided calibrated ages around 730 B.C. to A.D. 50 years for the loess layer (horizon '2'). The base of that loess is made up of a solifluction horizon constituting a shear plane during cold phases; and close to the fault, this horizon includes an old sample (> 20 ky B.C.) very probably reworked from an eroded Upper Pleistocene layer. A vertical separation of this layer of about 50 cm is observed along the fault plane that cuts the loess (layer '2') and is sealed by the modern soil (Fig. 11). Considering the fault dip and the slip vector of the fault, as evidenced by striations with a 25° pitch on the fault plane, a simple calculation reveals a minimum slip of ca. 1.5 m during one single event. Applying classical empirical relationships (Wells and Coppersmith, 1994), this calculated displacement for all earthquake fault types provides a magnitude $M_w = 6.8$ to 7.1 ± 0.3 , either considering the 1.5 m as a maximum or a mean value respectively. We also notice that the loess material is incorporated in a thick fault gouge, a zone of intense deformation, consequently implying that the late Holocene deposits are affected by faulting. This trench reveals one surface faulting event, consistent with a magnitude M_w around 7 that occurred probably during the 380 B.C. and A.D. 670 time span (covering the possible ages of samples

gathered at the base of the soil and at the top of the loess layer). In an additional small trench on the other side of the mini-graben, we found a granitic basement that is severely sheared and deformed in a fault zone located almost in the center of the trench. The displacement of the fault observed is around 20-25 cm and affects the base of the present-day soil (Fig. 11). Our dating places the event between 835 B.C. and A.D. 995: this could reasonably correspond to the event in T1. Another trench between trench-2 and trench-2' did not reveal any tectonic deformation because it was placed between the two faults bounding the graben-like depression, and it is not described here.

4.5. Northern area (*Predgornoje*) trenches

The last paleoseismological investigations were performed in the *Predgornoje* area (7-12 September 2015) (Fig. 1). The two sites were selected based on two lineaments that were perceptible in the morphology northeast of the river and southwest on the Tavia Hills (Fig. 8).

Trench-3 location was selected after a field inspection in the western continuation of the northern lineament. This latter may be largely controlled by lithological contrast; however, an abandoned pit, just 1.5 km south of *Predgornoje* village along the right bank of the Irtysh River, revealed a clear deformation zone in the loess deposit (Fig. 12). We then cleaned, logged, and interpreted this outcrop (see supplementary material for pictures). Trench-4 location was chosen on the basis of a morphological analysis that pointed out the occurrence of a large N115°E trending scarp along the northeastern slope of the Tavia Hills, a kind of basement hinterland that overlooks the Irtysh alluvial plain (Fig. 8 and 13, plus sketch in supplementary material). Suspecting the occurrence of a pressure ridge in the basement (Fig. 13), we planned to dig a perpendicular trench at the tip of this ridge, in the overlying alluvial fan deposits. Unfortunately, the excavator suffered a definitive break that did not allow us to completely cross the structure.

Trench-3 is very informative with respect to the Irtysh Fault system activity. The section is 20 m long, over 3-4 m high, and exhibits a thick and faulted layer of loess (layer '3') and wedge shaped soil

horizon (layer '2') (Fig. 12). The fault kinematics are visible on a slickenside in the loess, mainly normal with a dextral component (fault plane striking N98°E, dipping 72° to the north; striation dipping 75° to the east). At the base of the section, the internal stratigraphy of the loess layer is disturbed: gravel and soil interbeds are folded, overturned, disrupted. We speculate that those features could correspond to soft-sediment deformation. The possible causative shaking event would have occurred after the formation of the soil (sample 3: 90 B.C.-A.D. 50) that was later deformed and before the deposition of the overlying cap (layer '2'). This overlying colluvium facies, which seals the fault and pinches out toward the footwall, is a relevant marker of a deformation event. This colluvial wedge includes loess clasts from the lower unit and is interpreted as an earthquake fault free-face degradation horizon deposited after the event. We have no direct access to the event-related offset. However, we use the colluvial wedge thickness as an indirect indicator of per-event displacement (McCalpin, 2009). In that case, a maximum thickness of 0.5 m leads to a 1-m-high scarp associated with an $M_w = 6.6-6.8$ earthquake. The event is interpreted to be older than the A.D. 425-600 age obtained for the older sample.

Trench-4, to the south, also provided information on recent deformation. It was excavated in alluvial fan deposits at the tip of the basement ridge suspected to represent the surface expression of a strike-slip fault. Actually, this short trench (10 m long) revealed that the late Pleistocene loess deposit (26,935-26,615 B.C.), then alluvial fan gravels and silts (6075-6010 B.C.) are affected by a kink-like fold, with minor secondary faulting with ≈ 5 to 10 cm normal offset (Fig. 13). Our interpretation is that this is evidence of the surface expression of a buried fault associated with the major strike-slip segment. The trench very probably did not touch the main fault; however, we state that the measured vertical separation of the alluvial fan base (25 cm) could be of coseismic origin and that it is used as a proxy to evaluate the paleoevent magnitude. The assumed 25-cm vertical offset could then be caused by a magnitude $M_w = 6.3 \pm 0.2$ single surface rupturing event that occurred after 6010 BC.

5. Discussion and Perspectives

5.1. *Map of active fault strands*

The map of active fault strands along the IFZ is drawn based on the morphotectonic and geological data described above, correlating them as much as possible with the existing basement fault map (Fig. 14). This proposed map has to be considered with caution as a first attempt toward a complete fault map useful in seismic hazard analyses.

The analysis of satellite images was undertaken all along the fault zone area between Podgornoje and Alibay; and several additional anomalies are suspected to be traces of active faulting, such as north of Ermanovka (right-lateral deflections), or near the Qasim-Qaysenov village (ponds along structural features), or around Alibay (linear scarps across alluvial deposits and deflections). We also use the location of the main accumulation zones of late Quaternary sediments around Öskemen and Predgornoje as indicators of possible pull-apart basins between two right-stepping right-lateral fault traces. Fault traces that display no morphological evidence of activity are not classified as active in this study.

Using the criteria above, we define a set of subparallel or branching fault portions (Fig. 14), with length between ~100 (Alibay-Bukhtarma) and 50 km (Ermanovka-Öskemen and Öskemen-Predgornoje). For the last two (Qasim-Qaysenov and north Predgornoje), we could gather only limited information on their lateral extension, because of the poor morphological signal and the lack of time to investigate them in the field.

5.2. *Earthquake timing and magnitude of paleoearthquakes*

A significant conclusion of the reconnaissance work is that several surface faulting events occurred during the Holocene, with possible magnitudes from 6.5 to more than 7, along various fault sections included in the inherited IFZ structure. The three largest segments are able to host those $M > 6.5$ paleoearthquakes as observed in their respective trenches, given their lengths. In one spot, we

could show a recurrence of two surface-rupturing events on a secondary fault section (Trench-1), which seems to have broken separately from the main structure (see Railway cut) only about 1 km away.

We are aware that bulk soil dating of the whole set of samples is a limiting factor to the accuracy of our results and interpretations. Keeping this in mind, we nonetheless underline that most of the activity is concentrated during a short time span of 3 ky during the late Holocene (Fig. 15). Certainly, we do not have either a sufficient data set of past large earthquakes in the area, on the IFZ or other faults in the same context, to fully describe their recent seismic history. However, in trench-2 and trench-4, where sediments date back to ~15-20 ky, paleoearthquake evidence is concentrated within a short time period of 3-4 ky at the end of the Holocene. There are many potential pitfalls to this reasoning, and the primary one could be the completeness of stratigraphic record. However, our case study seems to follow a behavior rather similar to that of other fault zones, as in the eastern Australian case with fault sets and clusters of earthquakes (Clark et al., 2017). Some recent papers tend to question the classical '*seismic cycle concept*' for intraplate faults in stable continent regions, concluding that major earthquakes are there episodic, clustered, and/or migrating (Calais et al., 2016; Liu et al., 2011; Stein et al., 2017). According to these new studies and resulting concepts, we should be careful in using a single slip rate value all along the fault slip history for seismic hazard studies. However, in this very preliminary stage of the IFZ study, we compile the data set covering two different time spans and propose a unique value for the whole structure over the late Pleistocene to Holocene.

5.3. *Slip rates and contribution of the geomorphological data*

Based on radiometric dating in one of the trenches, we could determine a slip rate value at only one site for the late Holocene time span, on a secondary fault 1 km south of the major structure. We try, in this section, to deliver supplementary data to this critical parameter of earthquake sources,

thanks to landscape feature offsets, covering a larger time span ($\gg 10$ ky). We use the small-scale bedrock-incised channels along the major fault scarp and regional morphoclimatic information.

According to Chlachula (2010), the drainage network has been set up in eastern Kazakhstan from the middle Pleistocene on (last 700 ky). The large-scale features, such as the Irtysh River and its network of tributaries, including the asymmetrical large alluvial fans shown in Figs. 3 and 4, could have been generated at that time when the climatic conditions became colder. Hills and low mountains are today crossed by a dense network of small-scale bedrock-incised creeks and channels and especially those cutting through the fault-related mountain range front along the IFZ. We assume that these incisions are the evidence of the last incision phase in the bedrock. To date, we have no direct radiometric or cosmogenic dating to place accurately the start of those incisions that trench into the mountain range front, and we can only provide a rough estimate to determine the rate of lateral offset of those features. Most of them have been hydrologically inactive during the current interglacial phase (Holocene), and we first state that they are older than the Holocene and associated with the peak during the major Last Glacial Maximum. During cold phases, this region of low elevation (i.e., all the sites investigated here like the Bukhtarma Reservoir area, Öskemen, Predgornoje) has been free of ice. It was, however, in the proximal neighborhood of glaciers (especially in this western region of the Altai Mountains) where the late Pleistocene ice caps prograded into basins (Lehmkuhl et al., 2004). Glacial periods are not prone to fluvial activity and bedrock incision because of cold and dry continental climatic conditions and of the spreading of permafrost in Central Asia (cryo-aridisation) (Sheinkman, 2011), but transitions to cooler phases are characterized by intense water flow because of abundant precipitations and sparse vegetation that favored runoff. The major Last Glacial Maximum is not synchronous in the world; and according to several authors (Ehlers et al., 2011; Lehmkuhl et al., 2004), the MIS 4 was probably the most pronounced cold period in the Central Asia ranges (Pamir, Tien Shan, Altai) after the MIS 5 ultimate interglacial period (Burgette et al., 2017; Zech, 2012). Our conclusion is that those small-scale bedrock-incised creeks that dissect the major fault scarp of the central southeastern area

(Bukhtarma) could date back to climate changes around this MIS 4 glacial stage (i.e., around 60 or 80 ky). They have probably been active during later phases such as MIS 2 as well.

Considering the various right-lateral deflections that could be measured along the fault strands, we compile the mean value at each point where a deflection could be observed, resulting in 25 deflection observations that are distributed within 10-m-spaced classes from 0 to 150 m. The observed deflections are mainly representative of the southeast central (Bukhtarma) section and the northwest central (Öskemen) area (see map in supplementary material). We briefly analyze the statistics, taking into account the reliability of the observations to avoid any bias in estimating a preliminary slip rate from those morphological data, based on the age hypothesis exposed before. The mean value of deflection is 47 m; the 50% percentile is 32 m (see supplementary material). The distribution shows a major mode centered around 25-30 m that we also find to be the most reliable features and the most constrained measurements. We suggest that this 25-30 m mode could represent the cumulative displacement as the last incision phase that we estimate dates back to 60-80 ky based on regional correlations, whereas the highest value would reflect displacements on larger time scale(s). With these hypotheses, we estimate a rough right-lateral slip rate in the range 0.3 to 0.5 mm/y. We spread this value to the whole fault system, which is another strong hypothesis because slip rate can vary along strike (e.g., Farbod et al., 2016; Solaymani Azad et al., 2015). We also acknowledge that this estimation is highly uncertain, being based on still poorly constrained assumptions (e.g., correlation of morphological features and age of incision). Therefore, it must be considered with caution and needs to be checked with further additional studies. The available geodetic data (Zubovich et al., 2010) show no perceptible relative motion around the fault, beyond the error bars of GPS vectors (~ 0.5 mm/y). We state that the horizontal slip rate obtained after our morphological analyses (< 0.5 mm/y) is consistent with those constraints, and we conclude that the Irtysh fault is probably accommodating a small fraction of intraplate deformation within the Eurasian Plate.

Vertical slip rate assessment from paleoseismological analysis across a secondary fault (0.22 mm/y) and horizontal component from morphological estimate for the main segment (0.3-0.5 mm/y) are consistent values. They should be cumulated to provide a geological rate for the fault zone.

6. Conclusion

The primary conclusion of this study is that the Irtysh fault, an old structure developed during Paleozoic times, is active and potentially caused large earthquakes during the Holocene. In all sites, we have found no more than two paleoearthquake events in the last 10,000 years. The observed displacements range between 0.25 and 1.5 m, suggesting events with magnitudes from Mw 6 to 7. No surface displacements consistent with larger earthquakes (Mw = 7.5 or higher) were seen. However, we stress that our investigations were not designed to detect purely horizontal slip, which could occur along the main fault trace. Vertical slip rate assessment for a secondary fault (0.22 mm/y) and horizontal component for the main segment (0.3-0.5 mm/y) are very preliminary and based on only a limited set of reliable data.

These conclusions are preliminary. The paleoseismological investigation presented provides only a glimpse of the complete picture. The evidenced active sections of the Irtysh fault are distributed onto a dense network of basement faults, and we probably only mapped a part of the active parallel and branching segments. With such possibly limited information, we may have also missed events in the time record because successive ruptures have jumped from one segment to another (see Klinger et al., 2005, for an example). This implies that, for one specific event, total offsets may be larger than observed, and then event magnitude underestimated.

Despite the large uncertainties in our results, either in the proposed active fault map or in the quantification of earthquake magnitudes and timing, they positively recognize the Irtysh fault as a major active crustal structure inside the Kazakh cratonic region. The horizontal slip rate obtained from our morphological analyses (< 0.5 mm/y) is consistent with the geodetic constraints that show

no perceptible relative motion around the fault, beyond the error bars of GPS vectors (~ 0.5 mm/y). However, we conclude from our long-term tectonics study that the Irtysh fault is accommodating a fraction of the ~ 1 mm/y shortening that is probably absorbed in the stable Eurasia, within the Kazakh platform north of the Tien Shan.

Further studies are obviously required and strongly recommended before sound conclusions can be drawn in terms of earthquake hazard.

7. Acknowledgments

The authors acknowledge Dr. Christoph Grützner and an anonymous reviewer for their comments and suggestions, which significantly improved the manuscript.

8. References

- Arrowsmith, J.R., Crosby, C.J., Korzhenkov, A.M., Mamyrov, E., Povolotskaya, I., Guralnik, B., Landgraf, A., 2017. Surface rupture of the 1911 Kebin (Chon–Kemin) earthquake, Northern Tien Shan, Kyrgyzstan. *Geol. Soc. Lond. Spec. Publ.* 432, 233–253. <https://doi.org/10.1144/SP432.10>
- Bekzhanov, G.R., Koshkin, V.Y., Nikitchenko, I.I., 2000. Geological setting of Kazakhstan at 1/500,000; sheets L-44-A; L-44-B; L-45-A; M-44-A; M-44-B; M-44-G; M-45-A.
- Burgette, R.J., Weldon, R.J., Abdrakhmatov, K.Y., Ormukov, C., Owen, L.A., Thompson, S.C., 2017. Timing and process of river and lake terrace formation in the Kyrgyz Tien Shan. *Quat. Sci. Rev.* 159, 15–34. <https://doi.org/10.1016/j.quascirev.2017.01.003>
- Calais, E., Camelbeeck, T., Stein, S., Liu, M., Craig, T.J., 2016. A new paradigm for large earthquakes in stable continental plate interiors. *Geophys. Res. Lett.* 43, 10,621–10,637. <https://doi.org/10.1002/2016GL070815>
- Campbell, G.E., Walker, R.T., Abdrakhmatov, K., Schwenninger, J., Jackson, J., Elliott, J.R., Copley, A., 2013. The Dzhungarian fault: Late Quaternary tectonics and slip rate of a major right-lateral strike-slip fault in the northern Tien Shan region. *J. Geophys. Res. Solid Earth* 118, 5681–5698. <https://doi.org/10.1002/jgrb.50367>
- Campbell, G.E., Walker, R.T., Abdrakhmatov, K., Jackson, J., Elliott, J.R., Mackenzie, D., Middleton, T., Schwenninger, J.-L., 2015. Great earthquakes in low strain rate continental interiors: An example from SE Kazakhstan. *J. Geophys. Res. Solid Earth* 120, 5507–5534. <https://doi.org/10.1002/2015JB011925>
- Chlachula, J., 2010. Pleistocene climate change, natural environments and Palaeolithic occupation of East Kazakhstan. *Quat. Int.* 220, 64–87. <https://doi.org/10.1016/j.quaint.2009.09.011>
- Clark, D., McPherson, A., Cupper, M., Collins, C.D.N., Nelson, G., 2017. The Cadell Fault, southeastern Australia: a record of temporally clustered morphogenic seismicity in a low-strain intraplate region. *Geol. Soc. Lond. Spec. Publ.* 432, 163–185. <https://doi.org/10.1144/SP432.2>
- Dorbath, C., Van der Woerd, J., Arefiev, S.S., Rogozhin, E.A., Aptekman, J.Y., 2008. Geological and Seismological Field Observations in the Epicentral Region of the 27 September 2003 Mw 7.2 Gorny Altay Earthquake (Russia). *Bull. Seismol. Soc. Am.* 98, 2849–2865. <https://doi.org/10.1785/0120080166>
- Ehlers, J., Gibbard, P.L., Hughes, P.D., 2011. Introduction, in: *Developments in Quaternary Sciences*. Elsevier, pp. 1–14. <https://doi.org/10.1016/B978-0-444-53447-7.00001-5>
- Farbod, Y., Shabanian, E., Bellier, O., Abbassi, M.R., Braucher, R., Benedetti, L., Bourlès, D., Hessami, K., 2016. Spatial variations in late Quaternary slip rates along the Doruneh Fault System (Central Iran): QUATERNARY SLIP RATES ALONG THE DORUNEH FAULT SYSTEM. *Tectonics* 35, 386–406. <https://doi.org/10.1002/2015TC003862>
- Ghose, S., Mellors, R.J., Korzhenkov, A.M., Hamburger, M.W., Pavlis, T.L., Pavlis, G.L., Omuraliev, M., Mamyrov, E., Muraliev, A.R., 1997. The MS = 7.3 1992 Suusamy, Kyrgyzstan, earthquake in the tien shan: 2. Aftershock focal mechanisms and surface deformation. *Bull. Seismol. Soc. Am.* 87, 23–38.
- Glorie, S., De Grave, J., Delvaux, D., Buslov, M.M., Zhimulev, F.I., Vanhaecke, F., Elburg, M.A., Van den haute, P., 2012. Tectonic history of the Irtysh shear zone (NE Kazakhstan): New constraints from zircon U/Pb dating, apatite fission track dating and palaeostress analysis. *J. Asian Earth Sci.* 45, 138–149. <https://doi.org/10.1016/j.jseaes.2011.09.024>
- Grützner, C., Walker, R.T., Abdrakhmatov, K.E., Mukambaev, A., Elliott, A.J., Elliott, J.R., 2017. Active Tectonics Around Almaty and along the Zailisky Alatau Ranges: Active Tectonics Around Almaty Ranges. *Tectonics* 36, 2192–2226. <https://doi.org/10.1002/2017TC004657>
- Klinger, Y., Xu, X., Tapponnier, P., Van der Woerd, J., Lasserre, C., King, G., 2005. High-Resolution Satellite Imagery Mapping of the Surface Rupture and Slip Distribution of the Mw 7.8, 14

- November 2001 Kokoxili Earthquake, Kunlun Fault, Northern Tibet, China. *Bull. Seismol. Soc. Am.* 95, 1970–1987. <https://doi.org/10.1785/0120040233>
- Kreemer, C., Blewitt, G., Klein, E.C., 2014. A geodetic plate motion and Global Strain Rate Model. *Geochem. Geophys. Geosystems* 15, 3849–3889. <https://doi.org/10.1002/2014GC005407>
- Lehmkuhl, F., Klinge, M., Stauch, G., 2004. The extent of Late Pleistocene glaciations in the Altai and Khangai Mountains, in: *Developments in Quaternary Sciences*. Elsevier, pp. 243–254. [https://doi.org/10.1016/S1571-0866\(04\)80130-1](https://doi.org/10.1016/S1571-0866(04)80130-1)
- Liu, M., Stein, S., Wang, H., 2011. 2000 years of migrating earthquakes in North China: How earthquakes in midcontinents differ from those at plate boundaries. *Lithosphere* 3, 128–132. <https://doi.org/10.1130/L129.1>
- Lunina, O.V., Gladkov, A.S., Novikov, I.S., Agatova, A.R., Vysotskii, E.M., Emanov, A.A., 2008. Geometry of the fault zone of the 2003 Ms=7.5 Chuya earthquake and associated stress fields, Gorny Altai. *Tectonophysics* 453, 276–294. <https://doi.org/10.1016/j.tecto.2007.10.010>
- McCalpin, J. (Ed.), 2009. *Paleoseismology*, 2nd ed. ed, International geophysics series. Academic Press, Burlington, MA.
- Molnar, P., Qidong, D., 1984. Faulting associated with large earthquakes and the average rate of deformation in central and eastern Asia. *J. Geophys. Res. Solid Earth* 89, 6203–6227. <https://doi.org/10.1029/JB089iB07p06203>
- Petrov, O.V., Shuwen, D., Kiselev, E.A., Morosov, A.F., 2016. Atlas of geological maps of Asia and adjacent areas. International project. VSEGEI Publishing House.
- Reimer, P.J., Bard, E., Bayliss, A., Beck, J.W., Blackwell, P.G., Ramsey, C.B., Buck, C.E., Cheng, H., Edwards, R.L., Friedrich, M., Grootes, P.M., Guilderson, T.P., Hafliðason, H., Hajdas, I., Hatté, C., Heaton, T.J., Hoffmann, D.L., Hogg, A.G., Hughen, K.A., Kaiser, K.F., Kromer, B., Manning, S.W., Niu, M., Reimer, R.W., Richards, D.A., Scott, E.M., Southon, J.R., Staff, R.A., Turney, C.S.M., van der Plicht, J., 2013. IntCal13 and Marine13 Radiocarbon Age Calibration Curves 0–50,000 Years cal BP. *Radiocarbon* 55, 1869–1887. https://doi.org/10.2458/azu_js_rc.55.16947
- Rizza, M., Ritz, J. -F., Prentice, C., Vassallo, R., Braucher, R., Larroque, C., Arzhannikova, A., Arzhannikov, S., Mahan, S., Massault, M., Michelot, J. -L., Todbileg, M., ASTER Team, 2015. Earthquake Geology of the Bulnay Fault (Mongolia). *Bull. Seismol. Soc. Am.* 105, 72–93. <https://doi.org/10.1785/0120140119>
- Safonova, I., 2014. The Russian-Kazakh Altai orogen: An overview and main debatable issues. *Geosci. Front.* 5, 537–552. <https://doi.org/10.1016/j.gsf.2013.12.003>
- Sheinkman, V.S., 2011. Glaciation in the High Mountains of Siberia, in: *Developments in Quaternary Sciences*. Elsevier, pp. 883–907. <https://doi.org/10.1016/B978-0-444-53447-7.00065-9>
- Sloan, R.A., Jackson, J.A., McKenzie, D., Priestley, K., 2011. Earthquake depth distributions in central Asia, and their relations with lithosphere thickness, shortening and extension: Earthquake depth distributions in central Asia. *Geophys. J. Int.* 185, 1–29. <https://doi.org/10.1111/j.1365-246X.2010.04882.x>
- Smith-Konter, B.R., Sandwell, D.T., Shearer, P., 2011. Locking depths estimated from geodesy and seismology along the San Andreas Fault System: Implications for seismic moment release. *J. Geophys. Res.* 116. <https://doi.org/10.1029/2010JB008117>
- Solaymani Azad, S., Philip, H., Dominguez, S., Hessami, K., Shahpasandzadeh, M., Foroutan, M., Tabassi, H., Lamothe, M., 2015. Paleoseismological and morphological evidence of slip rate variations along the North Tabriz fault (NW Iran). *Tectonophysics* 640–641, 20–38. <https://doi.org/10.1016/j.tecto.2014.11.010>
- Stein, S., Liu, M., Camelbeeck, T., Merino, M., Landgraf, A., Hintersberger, E., Kübler, S., 2017. Challenges in assessing seismic hazard in intraplate Europe. *Geol. Soc. Lond. Spec. Publ.* 432, 13–28. <https://doi.org/10.1144/SP432.7>
- Wells, D.L., Coppersmith, K.J., 1994. New empirical relationships among magnitude, rupture length, rupture width, rupture area, and surface displacement 974–1002.

- Zech, R., 2012. A late pleistocene glacial chronology from the Kitschi-Kurumdu Valley, Tien Shan (Kyrgyzstan), based on ¹⁰Be surface exposure dating. *Quat. Res.* 77, 281–288. <https://doi.org/10.1016/j.yqres.2011.11.008>
- Zubovich, A.V., Wang, X., Scherba, Y.G., Schelochkov, G.G., Reilinger, R., Reigber, C., Mosienko, O.I., Molnar, P., Michajljow, W., Makarov, V.I., Li, J., Kuzikov, S.I., Herring, T.A., Hamburger, M.W., Hager, B.H., Dang, Y., Bragin, V.D., Beisenbaev, R.T., 2010. GPS velocity field for the Tien Shan and surrounding regions. *Tectonics* 29, n/a-n/a. <https://doi.org/10.1029/2010TC002772>

Figure captions

Fig. 1. General geological map of the IFZ area. Blue lines are all the faults traced from 1:500,000 geological maps of Russia (Bekzhanov et al., 2000); red lines locate the IFZ that is suspected or evidenced to be active, based on geomorphological and geological clues. Geological ensembles are modified from Safonova (2014). Upper left inset gives the general collisional context of the IFZ, well north of the collision front of the Himalaya (bold line with triangles); the western edge of the intraplate zone affected by collision-related deformation is characterized by large and low slip rate dextral faults, such as MA (Mongolia Altai fault). AT: Altyn Tagh, BR: Baikal rift, DL: Mongolian depression of lakes, KS: Kunlun Shan, QS: Qilian Shan, TB: Tunka basin, TS: Tien Shan.

Fig. 2. Seismic activity in the IFZ area (earthquake catalogue of the Institute of Geophysical Research of Kazakhstan, for the 1761-2015 time period). The map includes the GPS velocities of sites from Zubovich et al. (2010) of the area, in mm/y, with respect to fixed Eurasia. The distribution of earthquakes at depth (lower panel) is a proxy to the seismogenic depth (95% cutoff of cumulated distribution)

Fig. 3. Annotated satellite map of the southeastern Alibay area (see Fig. 1 for location along the fault zone), based on the satellite imagery available at http://services.arcgisonline.com/ArcGIS/rest/services/World_Imagery/MapServer. White arrows underline morphotectonic lineaments: their impact on topography and drainage network suggest a possible activation during the Quaternary. Bold grey contours represent the footprint of large Quaternary fan surfaces at the toe of the mountain range; the black arrows represent their asymmetry to the NW. The dot pinpoints a right-lateral deflection of the current incised channel (between 30 and 35 meters, depending on the selected piercing line). In supplementary material, we provide a morphological sketch of the area, to give rough and basic information about the topographic context and morphological background.

Fig. 4. Annotated satellite map of the central southeastern area (Bukhtarma) (see Fig. 1 for location along the fault zone), based on the satellite imagery available at ArcGIS Online. White arrows indicate morphotectonic lineaments: their impact on topography and drainage network suggest a possible activation during the Quaternary. Bold grey contours represent the footprint of large Quaternary fan surfaces at the toe of the mountain range; black arrows represent their asymmetry to the northwest. Black stars show the locations of the outcrop and trench described in this paper. In the supplementary material, we provide a morphological sketch of the area to give rough and basic information about the topographic context and morphological background.

Fig. 5. Zoom-in on the fault lineaments in the Bukhtarma area, illustrating the systematic dextral offset of small-scale bedrock-incised drainage on the major one to the northeast. White dashed contours represent the footprint of creek alluvial bottom, with a systematic dextral deflection of its erosion-protected downhill edge. Dots depict the right-lateral deflection values measured from satellite images; the range of values depends on the selected piercing lines. The southwestern lineament does not show any clear lateral deflection and could then only unveil a vertical motion.

Fig. 6: Morphological evidence of active tectonics in the central south Bukhtarma area (see Fig. 1 for location along the fault zone), nearby the cement plant. Top: The satellite image shows the remarkably linear mountain front at a change in bedrock geology with different erosional pattern on each side. Some drainage markers clearly prove the tectonic activation of this existing bedrock fault during the Quaternary, with for instance deflection of recent creek floors. Bottom: The landscape close to the cement plant is strongly influenced by the IFZ, with for instance this beheaded stream and this shutter ridge underlined by colluvium/scree dammed by the counter-slope scarp caused by faulting.

Fig. 7: Annotated satellite map showing morphological evidence of active tectonics in the central north area, southeast of Öskemen. Top: The landscape in the Central North area close to Öskemen strongly suggests active tectonics, with a large scarp partly controlled by lithological contrast. Large-

scale incised creeks are dextrally displaced (~45 to 165 m) on each side of this scarp (white arrows), suggesting a Quaternary activity. White dashed lines represent the contours of incised valley bottoms. Bottom: This satellite image shows an ~5-km-long lineament within a homogenous basement ensemble (amphibolites), with sparse indication of small-scale morphological features offsets (black dots with displacement values between 10 and 30 m). In the supplementary material, we provide morphological sketches of the area to give rough and basic information about the topographic context and morphological background.

Fig. 8: The satellite image covers the Irtys River and its alluvial plain. Morphological lineaments are sparse, only perceptible in the hills east of trench-3 site and in the Tavia hill east of trench-4 (white arrows).

Fig. 9 : Railway cut outcrop is evidence of the active tectonics along the shoreline of the Bukhtarma Reservoir. Top: View of the mountain range front toward the southeast, showing the slope break over several kilometers. The Railway cut ('trench') is found just behind the foreground slope edge, exactly at the knickpoint. Bottom: The Railway cut documents a fault between the bedrock (B) and Quaternary slope deposits (layers '3' and '4'). The youngest horizons ('1' and '2') are not faulted. Grid cells are 1 m x 1 m. See text for explanations.

Fig. 10: Trench-1 site. Top: Southward view of the secondary (with respect to the major fault evidenced at the Railway cut) E-W scarp (open red arrows) where trench-1 was dug and surveyed. Bottom: Simplified section of the eastern wall of trench-1 that documents the fault between the Holocene series and the bedrock. Ages are given in radiocarbon values (before calibration). See text for explanations.

Fig. 11 : Trench-2 site. Top: View to the northeast of the trench area, showing the mini-graben floor (white dashed line) and the actual drainage axis in the foreground. The two trenches (trench-2 and trench-2') were dug on each side of this structural feature. Middle: Simplified section of the

south-eastern wall of Trench-2. Bottom: Simplified section of the southeastern wall of trench-2', where a fault plane in the granite cuts into the Holocene soil and displaces its base. Faulting is affecting in both trenches up to ~2000-years-old deposits. Ages are given in radiocarbon values (before calibration). See text for explanations.

Fig. 12 : Trench-3 site. Top: A panoramic view of the sites area extending around the Irtysh River. The northern lineament is tenuous but can be inferred from reorientation of incisions and bench(es) in the slope. The southern lineament in the Tavia hill is more prominent (see Fig. 13). Bottom: Simplified section of the western wall of trench-3 highlighting the surface faulting in the Holocene loess deposits. The event horizon is suspected to include the modern soil material (1530 to 900 y BP). Ages are given in Radiocarbon values (before calibration). See text for explanations.

Fig. 13: Trench-4 site. Top: A view of the Tavia Hill and the morphotectonic feature that was detected before trenching, representing a basement ridge (in red) elongated in the N110° direction, which vanishes in the Irtysh alluvial plain. Middle: A view to the west in the axis of the basement ridge, which depicts the place where trench-4 was placed to investigate the interaction between alluvial fan deposits and the suspected fault. Bottom: Simplified section of the eastern wall of trench-3, which documents the alluvial deposits covering the Pleistocene loess layer. The base of this 7190-years-old (radiocarbon age) alluvium is deformed by warping and secondary faulting: this tiny deformation cannot be detected upward in this alluvium, maybe because of rotational accommodation in the gravels. Ages are given in radiocarbon values (before calibration). See text for explanations.

Fig. 14: Map proposing an active fault map of the Irtysh Fault System, based on morphological and trench data collected during this study. Yellow shaded surfaces represent potential subsiding volumes with accumulation of late Pleistocene/Holocene sediments (alluvium and loess) determined according to the geological map of Kazakhstan (Bekzhanov et al., 2000). Question marks are reported

when no information could be collected in the segment continuations; in other places, fault portion tips are figured out from the absence of clear morphological signal or significant change in strike.

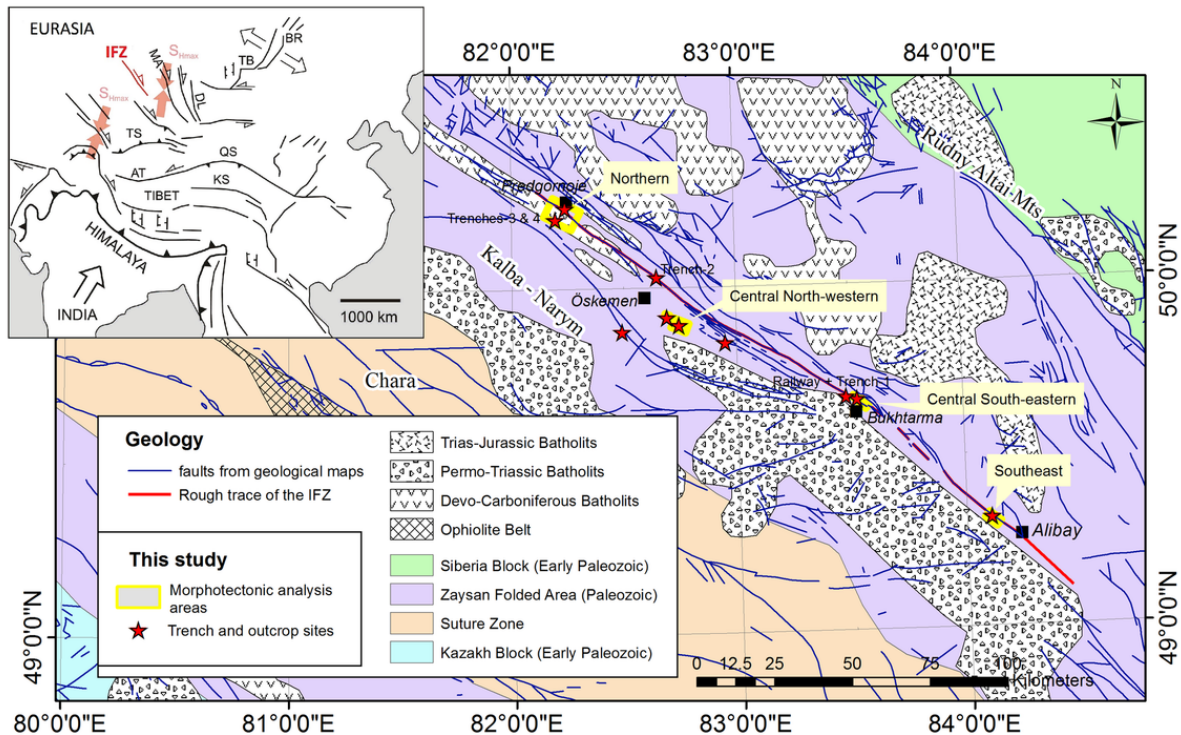
Fig. 15 : Chart illustrating the possible earthquake ages in the various studied outcrops and their potential correlation along the Irtysh Fault System. We infer surface-rupturing events between 2000 B.C and A.D. 500.

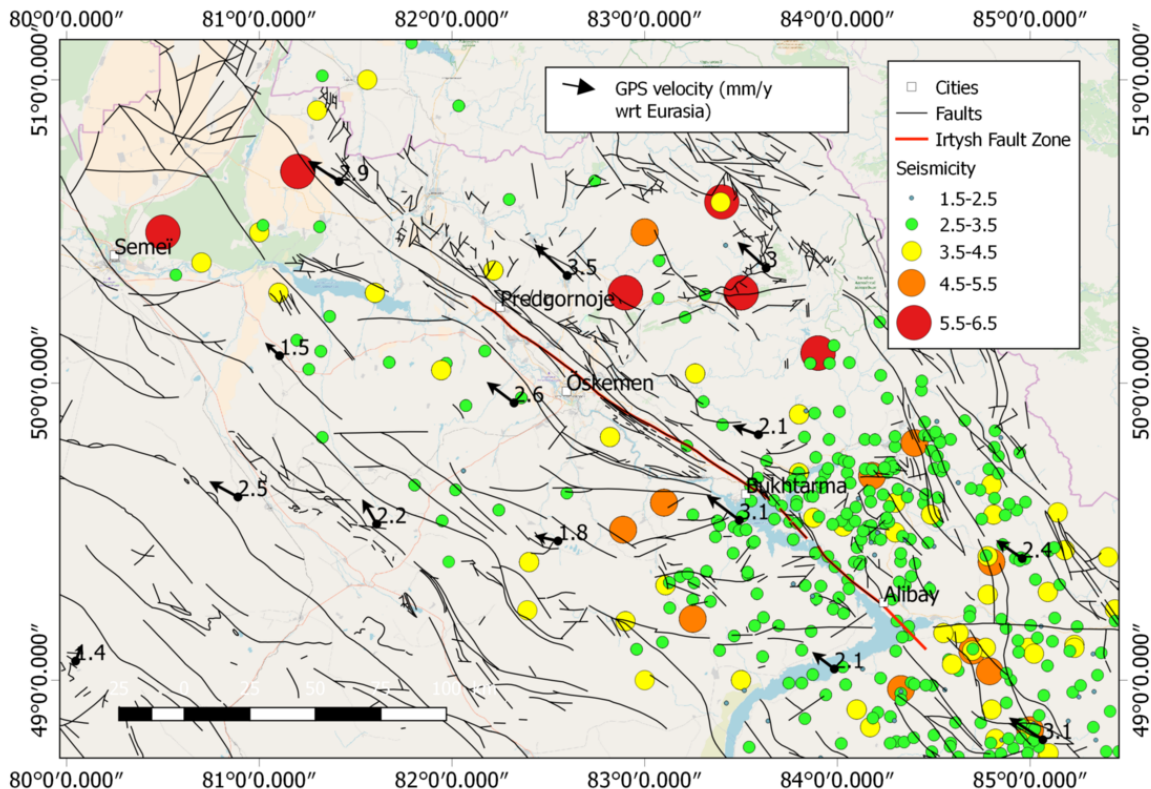
Table 1 : Coordinates of the studied outcrop and trenches.

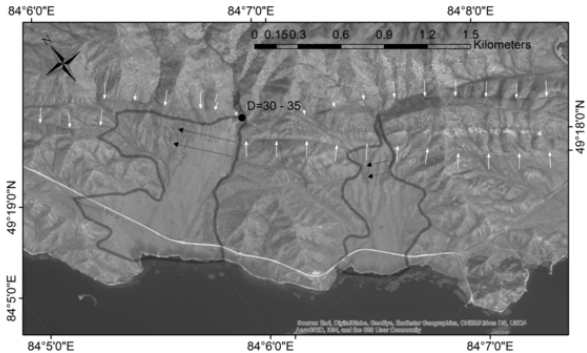
Site	Latitude N (°)	Longitude E (°)
Trench-1	49.67446	83.48202
Railway Cut	49.66720	83.53064
Trench-2	50.03108	82.64878
Trench-3	50.23332	82.24366
Trench-4	50.20071	82.19935

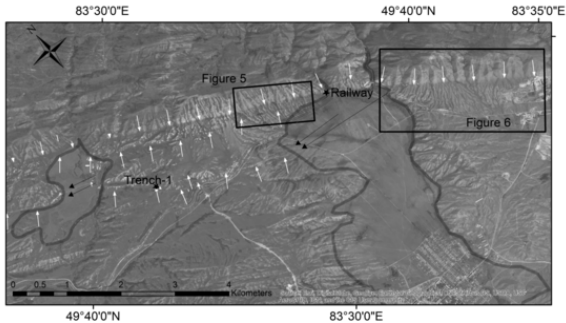
Table 2: Results of ¹⁴C datings. Radiocarbon and calibrated ages were provided by Beta Analytic. Samples are referred to their stratigraphic horizon (see text for description).

Exposure	N° sample	Stratigraphy ('n': layer – short description)	¹⁴ C Age (BP) and σ		Calibrated date - 2 σ (A.D.)	
Railway-Cut	1	'2' – Post-deformation colluvial layer	1,160	30	775	970
Railway-Cut	2	Base of '3' –colluvial wedge	2,940	30	-1,225	-1,045
Trench-1	1	'1' - non faulted soil	1,200	30	720	895
Trench-1	2	'1' - faulted soil	2,610	30	-815	-780
Trench-1	3	'2'	4,720	30	-3,630	-3,375
Trench-1	4	'3' – Base of colluvium	8,280	30	-7,455	-7,185
Trench-2	1	"2" - Base of faulted loess with basement clasts (footwall)	18,970	60	-21,030	-20,735
Trench-2	2	"2" - Top of faulted loess (footwall)	2,120	30	-340	-50
Trench-2	3	"1" - Base of non-faulted 'recent soil	1,600	30	395	540
Trench-2	5	"2" - Base of faulted loess with basement clasts (hanging wall)	2,400	30	-730	-400
Trench-2	6	"2" - Top of faulted loess (hanging wall)	2,220	30	-380	-200
Trench-2	7	"1" - Base of non-faulted 'recent soil	1,390	30	610	670
Trench-2'	1	'1" - faulted soil	2,650	30	-835	-795
Trench-2'	3	'1' - non faulted soil	1,110	30	885	995
Trench-3	1	'2' - colluvial wedge	1,530	30	425	600
Trench-3	2	'2' – very base of colluvial wedge	900	30	1,035	1,215
Trench-3	3	'3' – organic lens in loess	2,020	30	-90	55
Trench-4	1	'3' – faulted Pleistocene loess	24,690	100	-26,935	-26,615
Trench-4	2	'2' – alluvial fan deposits	7,190	30	-6,075	-6,010









83°31'0"E

